compounds. Martin (1970) and Fjeldly & Hanson (1974) observed that the elastic properties of the covalently bonded sphalerite-type and wurtzite-type compounds show a systematic tendency towards lattice instability as the ionicity increases. Koto & Schulz (1979) have reported that the diffuse scattering increases in intensity with increasing ionicity. The tendency toward the lattice instability should result in the increase in anharmonicity.

References

BACHMANN, R. & SCHULZ, H. (1984). *Acta Cryst.* A40, 668-675.
BEYELER, H. U., BRÜESCH, P., HIBMA, T. & BÜHRER, W. (1978). *Phys. Rev. B*, 18, 4570-4575.
BÜHRER, W. & BRÜESCH, P. (1975). *Solid State Commun.* 16, 155-158.
BÜHRER, W., NICKLOW, R. M. & BRÜESCH, P. (1978). *Phys. Rev. B*, 17, 3362-3370.
BURLEY, G. (1967). *Acta Cryst.* 23, 1-5.
CAVA, R. J., REIDINGER, F. & WUENSCH, B. J. (1977). *Solid State Commun.* 24, 411-416.
CAVA, R. J. & RIETMAN, E. A. (1984). *Phys. Rev. B*, 30, 6896-6902.
COCHRANE, G. (1967). *Br. J. Appl. Phys.* 18, 687-688.
FINGER, L. W. & PRINCE, E. (1975). *Natl. Bur. Stand. (US) Tech. Note* No. 854.
FJELDLY, T. A. & HANSON, R. C. (1974). *Phys. Rev. B*, 10, 3569-3577.
FRENKEL, J. (1926). *Z. Phys.* 35, 652-669.
International Tables for X-ray Crystallography (1974). Vol. IV. Birmingham: Kynoch Press. (Present distributor D. Reidel, Dordrecht, The Netherlands.)
JOHNSON, C. K. (1969). *Acta Cryst.* A25, 187-194.
JOHNSON, C. K. (1970). *Thermal Neutron Diffraction*, edited by B. T. M. WILLIS, ch. 9. Oxford: Clarendon Press.
KIHARA, K. & DONNAY, G. (1985). *Can. Mineral.* 23, 647-654.
KIHARA, K., MATSUMOTO, T. & IMAMURA, M. (1986). *Z. Kristallogr.* In the press.
KOTO, K. & SCHULZ, H. (1979). *Acta Cryst.* A35, 971-974.
MAIR, S. L. & BARNEA, Z. (1975). *Acta Cryst.* A31, 201-207.
MARTIN, R. M. (1970). *Phys. Rev. B*, 1, 4005-4011.
PHILLIPS, J. C. (1970). *Rev. Mod. Phys.* 42, 317-356.
PILTZ, R. O. & BARNEA, Z. (1987). *J. Appl. Cryst.* 20, 3-7.
SABINE, T. M. & HOGG, S. (1969). *Acta Cryst.* B25, 2254-2256.
SAKATA, M. & HARADA, J. (1976). *Acta Cryst.* A32, 426-433.
SCHULZ, H. & THIEMANN, K. H. (1977). *Solid State Commun.* 23, 815-819.
STEVENS, E. D. (1974). *Acta Cryst.* A30, 184-189.
STEVENSON, A. W. & BARNEA, Z. (1984). *Acta Cryst.* B40, 530-537.
STEVENSON, A. W., MILANKO, M. & BARNEA, Z. (1984). *Acta Cryst.* B40, 521-530.
WHITELEY, B., MOSS, G. & BARNEA, Z. (1978). *Acta Cryst.* A34, 130-136.
WILLIS, B. T. M. (1969). *Acta Cryst.* A25, 277-300.

Commensurate Ordering and Domains in the Ba₁.₂Ti₆.₈Mg₁.₂O₁₆ Hollandite

Commensurate Ordering and Domains in the $Ba_{1.2}Ti_{6.8}Mg_{1.2}O_{16}$ Hollandite

By ERIC FANCHON, JEAN VICAT, JEAN-LOUIS HODEAU, PIERRE WOLFERS, DUC TRAN QUI AND PIERRE STROBEL

Laboratoire de Cristallographie, Centre National de la Recherche Scientifique, Laboratoire associé à l'USMG, 166X, 38042 Grenoble CEDEX, France

Abstract

The $x = 1.20$ compound of $Ba_xTi_{8-x}Mg_xO_{16}$ hollandite has been investigated by electron microscopy and X-ray diffraction. Hollandites are formed of a framework providing tunnels in which the cations (here Ba^{2+}) are located. The competition between Ba/framework interactions and Ba/Ba repulsion leads to superstructure reflections, which can be incommensurable in the tunnel direction. The electron images show the occurrence of microdomains, and it was necessary to take them into account in X-ray refinements. The experimental data and least-squares results are: $M_r = 775.7$, monoclinic, $I2/m$, $a = 10.227$ (3), $b = 14.907$ (8), $c = 9.964$ (6) Å, $\beta = 90.77$ (4)°, $V = 1519$ (2) Å³, $Z = 5$, $D_x = 4.24$ Mg m⁻³, $\lambda(Ag\ K\alpha) = 0.5608$ Å, $\mu = 4.24$ mm⁻¹, $F(000) = 1796$, $T = 293$ K. Final $wR(F^2) = 0.05$ for 1776 unique reflections. The structure inside ordered domains is characterized by the $m_0 = 5$ $\cdots$Ba(1)-[Ba(1)-□-Ba(2)-□-Ba(1)]$\cdots$ sequence along the tunnels (□ = vacancy). The two adjacent Ba(1) cations are

displaced from the center of the cage toward the neighboring vacancy, as a result of Ba/Ba repulsion. A model is proposed in which small domains are included in a reference matrix. The domains are all made of the same Ba/□ sequence but translated with respect to the reference, the basic translation being the cell parameter b_{sub} of the subcell.

Introduction

Hollandite-type compounds obey the general formula $A_x(B_{8-y}B'_y)O_{16}$ with $x \leq 2$ (and y determined by charge balance). They are based on a framework of octahedrally coordinated B/B' cations, with A cations in tunnels parallel to the fourfold (or twofold) rotation axis of the tetragonal (or monoclinic) space group, c (or b) ≈ 3 Å. Because of this tunnel structure, they attracted interest as simple model systems for the study of some basic aspects of superionic conduction. The A site is a square-prismatic environment formed by O atoms. Its partial occupation generally leads to superlattice formation.

The compound $K_{1.54}Ti_{7.23}Mg_{0.77}O_{16}$ has recently been studied using various experimental techniques (X-ray diffraction, electron microscopy, ionic conductivity, NMR, specific heat measurements, Raman and IR scattering). X-ray rotation photographs (Beyeler & Schüler, 1980) showed diffuse streaks perpendicular to the tunnel direction, interpreted as a static short-range order of K^+ ions within the tunnels, the order in a given tunnel being uncorrelated with that in neighboring ones. Weber & Schulz (1983) refined its structure in the subcell assuming long-range one-dimensional order and found that the K^+ ions are displaced from the site center along the tunnel axis towards a vacancy by $0.24 c$ ($c = 2.97$ Å), a result consistent with a diffuse profile study (Beyeler, Pietronero & Strässler, 1980). This type of displacement was also found in $K_{1.33}Mn_8O_{16}$ (Vicat, Fanchon, Strobel & Tran Qui, 1986), in $K_{1.8}Sb_{5.55}Li_{2.45}O_{16}$ (Watelet, Besse, Baud & Chevalier, 1982) and in several minerals (Post, Von Dreele & Buseck, 1982). It originates in the electrostatic repulsion between mobile ions and is probably general. One exception recently reported is $Ag_{1.8}Mn_8O_{16}$, where Ag^+ ions were put (without refining displacement) at the center of the bottlenecks, in square-planar coordination (Chang & Jansen, 1986).

Some hollandite-type compounds exhibit a superstructure made of relatively sharp peaks. In this case, the tunnels are strongly correlated, resulting in a three-dimensional A-ion ordering. Intermediate cases of correlation between tunnels have also been reported (Mijlhoff, IJdo & Zandbergen, 1985; referred to hereafter as MIZ). $Ba_xTi_{8-x}Mg_xO_{16}$ is one of such three-dimensionally ordered hollandites. Electron diffraction and HREM imaging studies (Bursill & Grzinic, 1980; referred to as BG) revealed an incom-

mensurate superlattice ordering of Ba^{2+} ions in this series. According to BG, the x range is large ($0.8 \leq x \leq 1.33$), whereas the modulation propagation vector range is small ($2.35 \leq m \leq 2.965$, where m is the ratio between the modulation period p and the sublattice period b_{sub}). These authors used a microdomain model to explain the concurrent variations of x and m. No Ba^{2+} displacement was reported. BG proposed three structural models, including a disordered one, for the commensurate superstructure $Ba_{1.2}Ti_{6.8}Mg_{1.2}O_{16}$. Microdomains in HREM images were interpreted as due to the occurrence of the three proposed models in this compound.

We reinvestigated the Ba-ion ordering and the displacement in the $x = 1.20$ phase using high-resolution imaging and X-ray diffraction. The first technique confirms the occurrence of microdomains: this fact had to be taken into account for X-ray refinements. The problem of the x-value range is discussed, together with the various models used to describe these compounds (microdomains, modulation wave). We propose an alternative description of disorder in the $x = 1.20$ phase.

Experimental

Samples of $Ba_{1.2}Ti_{6.8}Mg_{1.2}O_{16}$ were prepared by direct synthesis from stoichiometric amounts of $BaCO_3$, TiO_2 and MgO. After initial heating at 1270 K to convert $BaCO_3$ to BaO, the oxide mixture was ground again, sealed in 5 mm diameter platinum tubes, rapidly heated to 1770 K for 10 h and then cooled at a rate of 5 K h^{-1} to 1070 K. This procedure gave hollandite-type crystals of various colors. Crystals of $Ba_{1.2}Ti_{6.8}Mg_{1.2}O_{16}$ are black, but more or less transparent depending on crystal thickness. Color is probably due to reduction of a fraction of Ti^{4+} into Ti^{3+} during firing. This fraction could not be determined by refinement because of the high correlations between the Ti/Mg ratio and the thermal factors. A small amount of orange or yellow crystals, with presumably different compositions, were found in the same run. D_m was not measured.

Electron diffraction studies were performed using a Philips electron microscope (120 kV) equipped with a side-entry double-tilt goniometer. Specimens were ground in an agate mortar and mounted on holey carbon films. These crystals and the single crystal used for X-ray data collection came from the same batch and had identical colors.

Whereas many hollandites have tetragonal symmetry, X-ray precession photographs show a small distortion in $Ba_{1.2}Ti_{6.8}Mg_{1.2}O_{16}$, giving a monoclinic cell with β close to 90° (a cause of frequent twinning). These photographs, together with electron diffraction patterns, show satellites in the b^* direction. Their position is generally not exactly commensurate with the hollandite sublattice ($q^* = 0.39 b^*$ for the sample

represented in Fig. 1). For black crystals the modulation propagation vector $\mathbf{q}^*$ ($=\mathbf{b}^*/m$) varies in the range $0.38-0.40\,\mathbf{b}^*$. The commensurate $\mathbf{q}^*=0.40\,\mathbf{b}^*$ superstructure ($m=2.5$) can be described with a centered five-cell supercell along the tunnel direction $\mathbf{b}$, whereas the periodicity is unaffected along a and c axes ($\mathbf{b}_{super}=m_0\mathbf{b}_{sub}$, $m_0=5$). Within this supercell the extinctions indicate the space group to be $I2/m$ $I2$ or Im. Dryden & Wadsley (1958) reported diffuse reflections in $Ba_xTi_{8-x}Mg_xO_{16}$ ($0.67<x<1.14$) and solved the average structure in space group $I4/m$ using Weissenberg films.

The X-ray data collection was performed on a four-circle Philips PW1100 diffractometer. A sample with a twin ratio less than 0.5% (evaluated from X-ray intensities) was selected and the lattice parameters were refined from θ values of 25 reflections over the range $20\le2\theta\le32°$. X-ray precession photographs and scans along $(0k0)$, $(1k1)$, $(\bar{2}k2)$, $(\bar{3}k1)$, $(0k2)$ and $(3k0)$, with $-10\le k\le10$, on the diffractometer did not show any significant deviation from the commensurate value $\mathbf{q}^*=0.40\,(1)\,\mathbf{b}^*$. The following measurement conditions were used: graphite-monochromated Ag $K\alpha$ radiation; $\theta/2\theta$ scan; scan speed $=0.06°\,s^{-1}$; scan width $\Delta\omega=1.5°$ for $\theta\le15°$ and $1.7°$ above; background measuring time equal to scan time; three standard reflections checked every 2 h.

3978 reflections of half the Ewald sphere ($l\ge0$) up to $(\sin\theta)/\lambda=0.89\,\text{Å}^{-1}$ were collected ($|h_{max}|=18$, $|k_{max}|=26$, $l_{max}=19$). Lorentz and polarization corrections were applied as well as a parallelepipedic absorption correction [sample defined by (100), (010), (001) faces and dimensions $0.144\times0.288\times0.080\,$mm along $\mathbf{a}$, $\mathbf{b}$ and $\mathbf{c}$, respectively]: max. and min. transmission coefficients are 0.7544 and 0.5565. After averaging equivalent reflections hkl and $h\bar{k}l$ and removing 116 reflections with $I_o\le\sigma(I_o)$, a final set

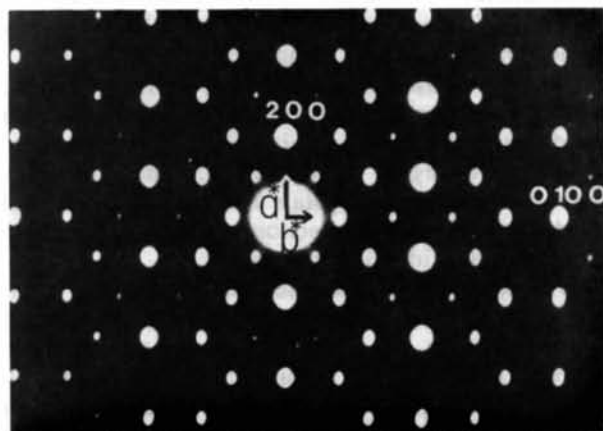Table 1. *Atomic coordinates and thermal factors* (*isotropic for* O, $U_{eq}=\frac{1}{3}\sum_iU_{ii}$ *for* Ba *and* Ti/Mg) *in the subcell with e.s.d.'s in parentheses*

	x	y	z	U_{eq}/U_{iso} (Å^2)
Ba(1)	0	0.3357 (2)	0	0.0115 (2)
Ba(2)	0	$\frac{1}{2}$	0	0.0215 (4)
Ti/Mg(1)	0.64721 (4)	0	0.16884 (4)	0.01154 (8)
Ti/Mg(4)	0.16532 (4)	0	0.34861 (4)	0.01137 (8)
O(1)	0.8428 (1)	0	0.1979 (1)	0.0096 (2)
O(4)	0.8428 (1)	0	0.4590 (2)	0.0112 (2)
O(7)	0.2048 (1)	0	0.1504 (1)	0.0098 (2)
O(10)	0.4587 (2)	0	0.1758 (2)	0.0115 (2)

of 1776 independent observations* was observed {internal reliability factor $r=[\sum_\mathbf{h}\sum_i|\langle F(\mathbf{h})\rangle-F_i(\mathbf{h})|]/\sum_\mathbf{h}\sum_iF_i(\mathbf{h})=1.7\%$, with $\langle F(\mathbf{h})\rangle=$ average of equivalent reflections}.

Structure determination

Data reduction, preliminary refinements and Fourier calculations were carried out with the *SDP* package (Enraf–Nonius, 1979), and subsequent 'non-standard' refinements with the *MXD* program (Wolfers, 1987). The latter were based on $I=|F|^2$ with $1/\sigma(I)^2$ weighting scheme (where σ is due to counting statistics).

All the results reported here were obtained with the *MXD* program on a VAX 780 computer. Atomic scattering form factors and anomalous f' and f'' factors were taken from *International Tables for X-ray Crystallography* (1974).

Refinement in the subcell

The structure was refined first in the subcell ($\mathbf{b}_{sub}=2.981\,\text{Å}$) using the 825 sublattice reflections (space group $I2/m$). Initial atomic coordinates of the framework atoms Ti/Mg and O in the $I2/m$ space group were determined from those of Mn and O in $K_{1.33}Mn_8O_{16}$ (Vicat *et al.*, 1986). We assume the Ti/Mg atom is the average $0.85\,$Ti$+0.15\,$Mg, which corresponds to $x=1.20$ stoichiometry and complete substitutional disorder. Two independent Ba positions were found in the tunnel (Fig. 4a): Ba(1) at $0,\frac{1}{2}-\delta y_{sub},0$ and Ba(2) at $0,\frac{1}{2},0$ (center of the square prism). Because of the overlapping of Ba atoms in this small cell, it was impossible to refine simultaneously δy_{sub}, Ba-site occupancies and Ba thermal factors. We therefore placed δy_{sub} in a separate diagonal block. Atomic coordinates, thermal parameters and agreement factors are given in Tables 1 and 2, line (a). The Ba(1) displacement is $0.496\,\text{Å}$. The occupancy-factor values $p[Ba(1)]=0.197\,(1)$ and

Fig. 1. Electron diffraction pattern of the [001] zone of $Ba_{1.2}Ti_{6.8}Mg_{1.2}O_{16}$.

Table 2. *Results of the different refinements (based on $|F|^2$, with 1776 independent reflections in the supercell)*

$$\chi^2 = 1/(n_{obs} - n_{param})\sum w(I_{obs} - I_{calc})^2.$$

	Positional parameters (and composition x when not fixed)	$wR(\%)$	$R(\%)$	χ^2	Number of variables
(a) Subcell	$\delta y_{sub} = 0.1643\,(3)$ $x = 1.18\,(1)$	6.3	5.5	2.23	36
(b) Ordered model	$\delta y = 0.0261\,(2)$	29	35	32	60
(c) BG's disordered model	$y_{Ba(1)} = 0.0645\,(2)$ $y_{Ba(2)} = 0.3154\,(3)$	20	2.5	15.4	61
(d) Model with 8 occupancy factors	$\delta y = 0.0344\,(2)$ $x = 1.14\,(2)$	13	5	6.4	68*
(e) Model using sequence probabilities	$\delta y = 0.03264\,(8)$	13.4	5.2	7.0	62*

* Difference Fourier syntheses give $\Delta\rho = 1.6$ and 4.6 e Å^{-3} for refinements (d) and (e), respectively.

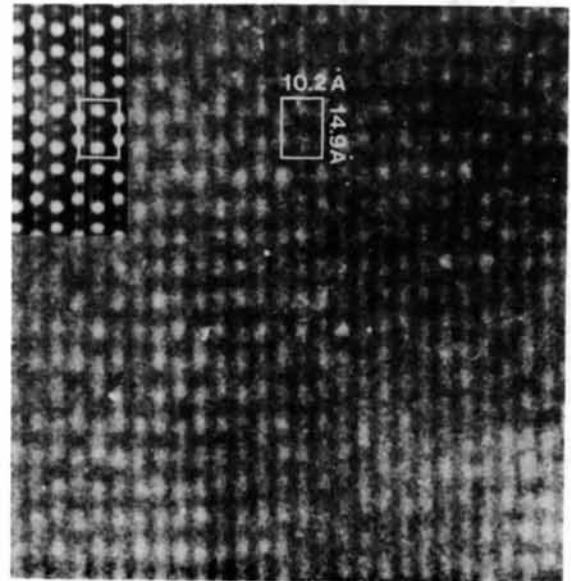$p[Ba(2)] = 0.196\,(2)$ confirm the $x = 1.20$ composition.

Refinement in the ordered supercell

In the following parts, the complete data set (1776 reflections) is used. The space group of the five-cell supercell was supposed to be $I2/m$. The framework-atom positions were deduced from the subcell ones. There are three Ba atoms distributed among the five sites of each tunnel. BG proposed for the Ba distribution in the tunnels one statistical disordered model and two ordered ones. In fact, the latter are identical, apart from an origin shift, and correspond to the sequence $\cdots$ Ba(1)–[Ba(1)–□–Ba(2)–□–Ba(1)]–$\cdots$ (□ = vacancy); the second tunnel of the cell is filled according to the I translation. Ba(1) is shifted from the center of the square-prismatic environment: $y_{Ba(1)} = 0.10 + \delta y$ (Fig. 4b). Refinements of positional and thermal parameters with the ordered model gave poor results (see Table 2, line b). The Ba(1) displacement is $\delta y = 0.0261\,(2)$, that is slightly different with $\delta y_{sub}/5 = 0.03286\,(6)$, found in the subcell. A difference Fourier synthesis gave peaks in the tunnel, showing that this ordered model is not satisfactory.
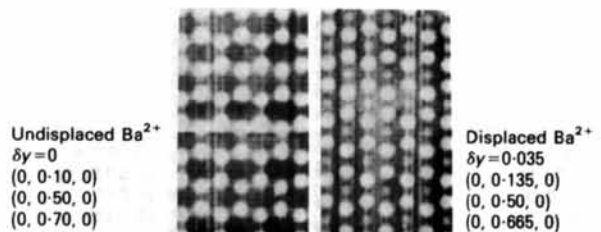
High-resolution images of the [001] zone and simulations

High-resolution imaging studies were performed using JEOL 200CX (200 kV) and Philips EM400 (120 kV) electron microscopes. The electron optical parameters for each microscope were: spherical aberration coefficients $C_s = 1.9$ and 2.8 mm, respectively; chromatic aberration $C_c = 1.8$ and 2.0 mm, respectively. Image simulations were drawn using the *SHRLI* suite of programs (O'Keefe, 1980) which is based on the Cowley–Moodie multislice model (Cowley & Moodie, 1957). The instrumental parameters C_s, α (the semi-angle of the incident illumination), and Δ (the r.m.s. focal spread) were checked by simulating images of a known test crystal LiTa$_3$O$_8$ (Hodeau, Marezio, Santoro & Roth, 1983), for which the image appearance rapidly changes with defocusing and variations in sample thickness.

Figs. 2(a) and 3(a) show high-resolution images ([001] zone) for Ba$_{1.2}$Ti$_{6.8}$Mg$_{1.2}$O$_{16}$ obtained with the Philips and JEOL microscopes, with an approximate structural resolution $d_s = 3.7$ and 2.7 Å, respectively. The edge of the same crystal was used to obtain these two images. As shown by BG, the main observation

(a)

Undisplaced Ba^{2+}
$\delta y = 0$
(0, 0.10, 0)
(0, 0.50, 0)
(0, 0.70, 0)

Displaced Ba^{2+}
$\delta y = 0.035$
(0, 0.135, 0)
(0, 0.50, 0)
(0, 0.665, 0)

(b)

Fig. 2. [001]-zone HREM images for Ba$_{1.2}$Ti$_{6.8}$Mg$_{1.2}$O$_{16}$ (Philips electron microscope). (a) Image; (b) simulations: $H = 50$ Å, $\lambda = 0.03349$ Å, $\alpha = 10^{-3}$ rad, $d_{lim} = 2.45$ Å, $C_s = 2.8$ nm, $\Delta = 275$ Å, $\delta f = -1000$ Å, plane (001).

is the row of bright blobs, separated by lines of dark intensity parallel to the tunnel direction **b**. The regularity of the blob sequence was broken at distances varying from 30 to 100 Å, indicating ordering in domains of limited size. These images were obtained on the crystal edge at Scherzer defocus; for such conditions and small thickness, white blobs correspond to vacancy positions. These white blobs are not equidistant on the Philips images (Fig. 2a). On the other hand, the JEOL image (Fig. 3a) shows a quasi-regular honeycomb pattern of white blobs in the ordered regions. The tunnel direction is visible even in the disordered regions.

Computations were then carried out to simulate the effect of various parameters. As shown by Pring, Smith & Jefferson (1983), image details with [001] zone change with defocusing and thickness; we also observed a contrast variation by introducing the opposite displacement δy of two successive Ba atoms (Ti and Mg are supposed to be disordered in the

(a)

Undisplaced Ba^{2+}
$\delta y = 0$
(0, 0·10, 0)
(0, 0·50, 0)
(0, 0·70, 0)

Displaced Ba^{2+}
$\delta y = 0·035$
(0, 0·135, 0)
(0, 0·50, 0)
(0, 0·665, 0)

(b)

Fig. 3. [001]-zone HREM images for $Ba_{1.2}Ti_{6.8}Mg_{1.2}O_{16}$ (JEOL electron microscope). (a) Image; (b) simulations: $H = 50$ Å, $\lambda = 0·02508$ Å, $\alpha = 10^{-3}$ rad, $d_{lim} = 2·0$ Å, $C_s = 1·9$ nm, $\Delta = 120$ Å, $\delta f = -750$ Å, plane (001).

supercell). Four examples of simulated images are given in Figs. 2(b) and 3(b); they correspond to simulations with the refined displacement $\delta y = \delta y_{sub}/5 = 0·035$ and without displacement. Although there is no large difference with respect to BG's simulation results (which included no Ba displacement), these patterns also show that an apparatus with resolution close to that required to separate successive Ba atoms gives electron images sensitive to the corresponding atomic displacements.

The superposition of the various ordered domains along the beam direction can explain the diffuse lines along the **b** axis between each ordered region. The width of these zones show that domain boundaries are not regular, neither parallel nor perpendicular to the tunnel direction. The domain size is variable and is a little larger than the regular blob-sequence length (but can be estimated on average at about 100 Å).

Introduction of disorder in the refinements

The high R values are mostly due to superstructure reflections, for which the observed intensities are smaller than the calculated ones. Therefore some disorder is present, which is consistent with observation of domains in HREM images. BG's disordered model $\frac{1}{2}Ba-[\frac{1}{2}Ba(1)-Ba(2)-\square-Ba-\frac{1}{2}Ba]$, in which we include two positional parameters $y_{Ba(1)}$ and $y_{Ba(2)}$, gives better results but is not yet satisfactory (Table 2, line c). We then consider eight independent sites in the supercell, with occupation factors labeled $s_1, \ldots, s_8$, located on the y axis: $0·10 - \delta y$, $0·10$, $0·10 + \delta y$, $0·30 - \delta y$, $0·30$, $0·30 + \delta y$, $0·50 - \delta y$, $0·50$, respectively. Using temperature factors $U_{displ}(i,j)$ and $U_{cen}(i,j)$ for the displaced and centered Ba atoms, respectively, this model requires only eight additional parameters. The results are greatly improved (see Table 2, line d), but yield $2(s_1 + s_2 + s_3 + s_4 + s_5 + s_6 + s_7) + s_8 = 2·85 (5)$ instead of 3 Ba atoms in the tunnel for the $x = 1·20$ composition.

A careful examination of site-occupancy values (Fig. 4c) led to the following assumption: the disorder is essentially due to defects that translate a given $Ba-[Ba-\square-Ba-\square-Ba]$ sequence with respect to the other ones. Various defects can interrupt the long-range order in the tunnels. The $Ba-[Ba-\square-Ba-\square-Ba]$ sequence is repeated after a defect, but translated with respect to the previous sequence. Each defect is characterized by the translation it induces. There are four such translations: $0·2\mathbf{b}_{super}$, $0·4\mathbf{b}_{super}$, $0·6\mathbf{b}_{super}$, $0·8\mathbf{b}_{super}$ that is $\mu \mathbf{b}_{sub}$ with $\mu = 1, 2, 3, 4$ (see Fig. 4d). The corresponding translations are labeled $T1$, $T2$, $T3$, $T4$. We include a fifth one, $T0$, corresponding to the reference sequence $\mu = 0$. In the microdomain hypothesis, if Γ is the full width at half maximum of the diffuse peaks, then the mean domain size is of the order of $1/\Gamma$. In our case, the domains are supposed small enough to give very diffuse peaks under
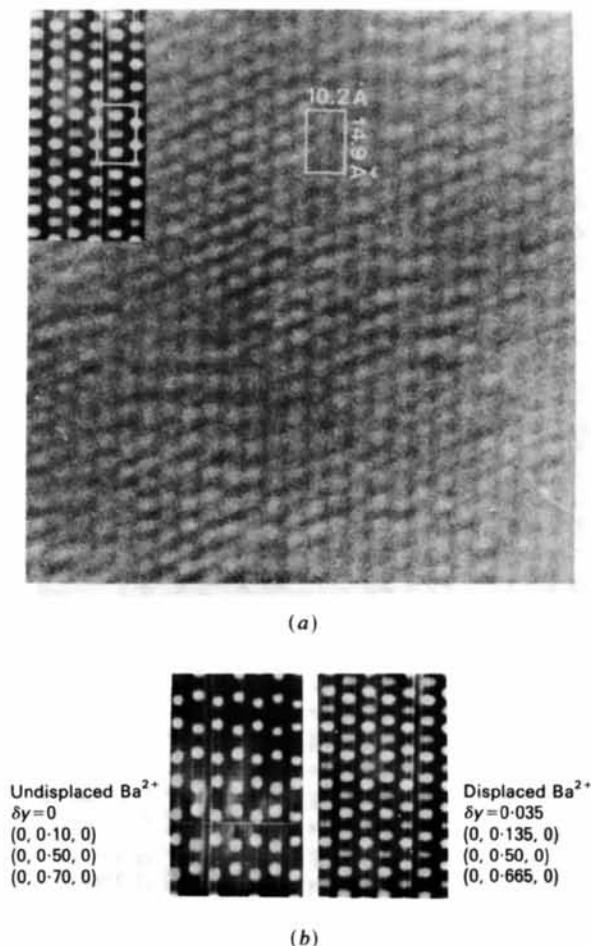
the Bragg reflections, so that we measured only the Bragg part. The integrated intensity is computed as follows: the total calculated structure factor is the sum of the structure factors of each individual. It is equivalent to use the structure factor F_0 of the ordered supercell (which includes the δy displacement) with phase factors $\exp(2\pi i \mu \, 0 \cdot 2k)$ for the five ($\mu =$ 0, 1, 2, 3, 4) sequences:

$$I(h, k, l) = S|n_0 + n_1 \exp(2\pi i \, 0 \cdot 2k)$$
$$+ n_2 \exp(2\pi i \, 0 \cdot 4k) + n_3 \exp(2\pi i \, 0 \cdot 6k)$$
$$+ n_4 \exp(2\pi i \, 0 \cdot 8k)|^2 \, |F_0(h, k, l)|^2.$$

The refined parameters n_0, n_1, n_2, n_3, n_4 (with the normalization condition $n_0 + n_1 + n_2 + n_3 + n_4 = 1$) give the corresponding proportions of the translated sequences. We found that $n_2 \simeq n_3$ and $n_1 \simeq n_4$ so that the m mirror is maintained on average. These two equalities were imposed as constraints in a subsequent refinement (Table 2, line e), which can be compared
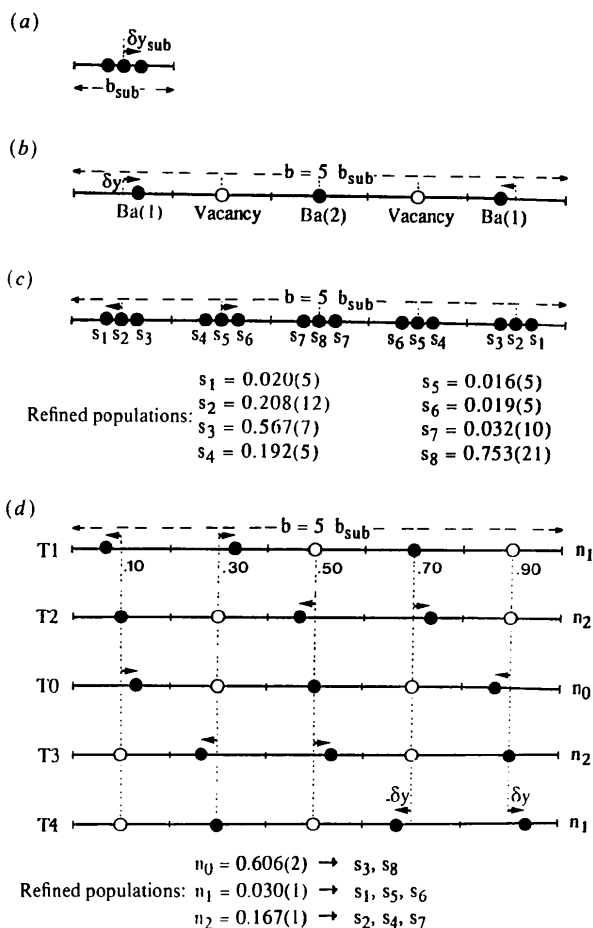
(a)

(b)

(c)

$$s_1 = 0.020(5) \qquad s_5 = 0.016(5)$$
Refined populations: $s_2 = 0.208(12) \qquad s_6 = 0.019(5)$
$$s_3 = 0.567(7) \qquad s_7 = 0.032(10)$$
$$s_4 = 0.192(5) \qquad s_8 = 0.753(21)$$

(d)

$$n_0 = 0.606(2) \rightarrow s_3, s_8$$
Refined populations: $n_1 = 0.030(1) \rightarrow s_1, s_5, s_6$
$$n_2 = 0.167(1) \rightarrow s_2, s_4, s_7$$

Fig. 4. Ba- and vacancy-ordering schemes in the tunnels: (*a*) Ba sites in the subcell (refinement *a* in Table 2); (*b*) body-centered $m_0 = 5$ supercell (refinement *b* in Table 2); (*c*) the 8 partially occupied Ba sites in the supercell (refinement *d* in Table 2); (*d*) the 5 translated sequences of $m_0 = 5$ multiplicity (refinement *e* in Table 2).

Table 3. *Atomic coordinates and thermal factors in the five-cell supercell with e.s.d.'s in parentheses [refinement* (*e*) *in Table* 2]

	x	*y*	*z*
Ba(1)	0	0·13264 (8)	0
Ba(2)	0	$\frac{1}{2}$	0
Ti/Mg(1)	0·6556 (5)	0	0·1630 (5)
Ti/Mg(2)	0·6428 (2)	0·1993 (3)	0·1779 (2)
Ti/Mg(3)	0·6474 (3)	0·4001 (2)	0·1629 (4)
Ti/Mg(4)	0·1580 (6)	0	0·3400 (5)
Ti/Mg(5)	0·1731 (2)	0·1993 (3)	0·3540 (2)
Ti/Mg(6)	0·1613 (4)	0·3999 (2)	0·3476 (4)
O(1)	0·845 (2)	0	0·195 (2)
O(2)	0·842 (1)	0·201 (1)	0·1974 (9)
O(3)	0·842(2)	0·4017 (8)	0·200 (2)
O(4)	0·851 (1)	0	0·461 (1)
O(5)	0·8449 (6)	0·200 (1)	0·4576 (7)
O(6)	0·8363 (8)	0·3989 (8)	0·460 (1)
O(7)	0·203 (2)	0	0·149 (3)
O(8)	0·2048 (9)	0·198 (1)	0·151 (1)
O(9)	0·206 (2)	0·4004 (8)	0·150 (2)
O(10)	0·462 (1)	0	0·169 (1)
O(11)	0·4573 (7)	0·201 (1)	0·1716 (6)
O(12)	0·459 (1)	0·3994 (8)	0·1838 (8)

Anisotropic thermal factors for Ba(1): $U_{11} = 0\cdot0133$ (4), $U_{22} = 0\cdot0180$ (6), $U_{33} = 0\cdot0146$ (4), $U_{13} = 0\cdot0006$ (3); and for Ba(2): $U_{11} = 0\cdot0183$ (7), $U_{22} = 0\cdot0171$ (8), $U_{33} = 0\cdot0173$ (7), $U_{13} = 0\cdot0005$ (5) Å^2. Global thermal factor for Ti/Mg: 0·0079 (1); and for O: 0·0090 (2) Å^2.

with the eight-site refinement merely by projecting the five shifted sequences on the **b** axis (Figs. 4*c,d*). The n_0, n_1, n_2 values are roughly in agreement with the eight site values obtained previously.

Table 3 gives atomic positions and thermal parameters for this last refinement. The δy value refined to 0·03264 (8), in agreement with the result of subcell refinement. This model requires only two additional independent parameters (three parameters n_0, n_1, n_2) constrained by the normalization condition), that is 62 instead of 60. It seems powerful since the wR and R factors with the ordered model decrease from 29 to 13·4% and from 35 to 5·2%, respectively. Moreover, the low standard deviation of the δy parameter and small size and small anisotropy of Ba thermal parameters indicate that this model is a good description of the Ba positions in the tunnel. $(\Delta/\sigma)_{max} = 0\cdot38$ for this last refinement.

Several subsequent checks were carried out:

(1) Refinements with individual isotropic thermal parameters for Ti/Mg and O atoms yielded oscillations larger than the standard deviations, and global parameters $U_{global}(Ti/Mg)$ and $U_{global}(O)$ had to be used. We attribute this to the difficulty of fully accounting for the disorder.

(2) Refinement of the six independent Ti/Mg ratios did not reveal any ordering. It should be noted that the crystallographic symmetry $I2/m$ does not allow one to predict a simple ordering of the Ti^{4+} and Mg^{2+} positions.

(3) Refinement in the less-symmetric $I2$ group did not lead to significantly better results.

(4) Refinement with extinction showed that this phenomenon is negligible.

Table 4. *Interatomic distances* (Å) *with e.s.d.'s in parentheses*

Ba(1)–Ba(1)	3·954 (3)		Ba(1)–Ba(2)	5·476 (3)
Ba(1)–O(1)	3·21 (4) ×2		Ba(2)–O(3)	2·96 (5) ×4
Ba(1)–O(2)	2·75 (5) ×2		Ba(2)–O(4)	3·61 (2) ×2
Ba(1)–O(6)	3·50 (2) ×2		Ba(2)–O(9)	2·97 (5) ×4
Ba(1)–O(7)	3·21 (4) ×2		Ba(2)–O(10)	3·31 (2) ×2
Ba(1)–O(8)	2·74 (5) ×2			
Ba(1)–O(12)	3·21 (2) ×2			
Ti/Mg(1)–O(1)	1·96 (3)		Ti/Mg(4)–O(4)	1·99 (2)
Ti/Mg(1)–O(3)	2·00 (1) ×2		Ti/Mg(4)–O(7)	1·97 (3)
Ti/Mg(1)–O(6)	1·94 (1) ×2		Ti/Mg(4)–O(9)	2·04 (2) ×2
Ti/Mg(1)–O(10)	1·98 (2)		Ti/Mg(4)–O(12)	1·93 (1) ×2
Average	1·97			1·98
Ti/Mg(2)–O(2)	2·04 (1)		Ti/Mg(5)–O(5)	1·89 (1)
Ti/Mg(2)–O(2)	1·95 (1)		Ti/Mg(5)–O(8)	2·05 (2)
Ti/Mg(2)–O(3)	1·94 (2)		Ti/Mg(5)–O(8)	1·97 (1)
Ti/Mg(2)–O(5)	2·03 (1)		Ti/Mg(5)–O(9)	1·93 (2)
Ti/Mg(2)–O(6)	2·02 (1)		Ti/Mg(5)–O(11)	2·01 (1)
Ti/Mg(2)–O(11)	1·90 (1)		Ti/Mg(5)–O(12)	2·03 (1)
Average	1·980			1·980
Ti/Mg(3)–O(1)	2·06 (2)		Ti/Mg(6)–O(6)	1·92 (1)
Ti/Mg(3)–O(2)	2·05 (1)		Ti/Mg(6)–O(7)	2·04 (2)
Ti/Mg(3)–O(3)	2·02 (2)		Ti/Mg(6)–O(8)	2·00 (1)
Ti/Mg(3)–O(4)	1·93 (1)		Ti/Mg(6)–O(9)	2·02 (3)
Ti/Mg(3)–O(5)	1·92 (1)		Ti/Mg(6)–O(10)	1·96 (1)
Ti/Mg(3)–O(12)	1·94 (1)		Ti/Mg(6)–O(11)	1·94 (1)
Average	1·987			1·980

Description of the structure

The interatomic distances and angles in the coordination polyhedra are listed in Table 4. The hollandite framework is built up of edge-sharing $(Ti/Mg)O_6$ octahedra forming double rutile-like chains (Byström & Byström, 1950). The five-cell supercell contains six of these independent octahedra. The structural refinement gave Ti/Mg-O distances in the range 1·89–2·06 Å, but the average Ti/Mg-O distance for each distorted octahedron varies from 1·98 to 1·97 Å only, in good agreement with the sum of the ionic radii $r(O^{2-}) = 1·38$ Å and the average $r(0·85 Ti^{4+} + 0·15Mg^{2+}) = 0·62$ Å (Shannon, 1976). These values are consistent with complete disorder of Ti/Mg.

The Ba-atom arrangement is now described as if it were fully ordered. Ba(2) is surrounded by eight O atoms at distances near 2·965 Å (4×2·96 and 4× 2·97 Å): the distances are not exactly equal because of the monoclinic deformation. There are four more O atoms at distances of 3·31 (×2) and 3·61 Å (×2) located in the direction of the center of the four lateral faces of the square prism. The Ba(1) shift along the tunnel makes its coordination polyhedron more irregular, with four short Ba-O distances near 2·745 Å, six long ones near 3·21 Å (see Table 4 and Fig. 5) and two additional O atoms at 3·50 Å. These sites resemble distorted cuboctahedra. The Ba-O contact distances calculated from Shannon's ionic radii in eightfold and twelvefold coordinations are 2·80 and 2·99 Å, respectively. It can be noted that the distance from the non-displaced Ba atom to the eight closest coordinating O atoms is typically 2·89 Å in

Mn hollandites (Post *et al.*, 1982), instead of 2·96 Å found here.

There are two independent Ba–Ba distances in the sequence ···–Ba(1)–[Ba(1)–□–Ba(2)–□–Ba(1)]–···: $d[Ba(1)–Ba(1)] = 3·954(3)$ and $d[Ba(1)–Ba(2)] = 5·476(3)$ Å. The corresponding Ba–Ba distances in $BaRu_6O_{12}$ ($x = 1·33$, $b_{sub} = 3·123$ Å) are 3·860 (3) and 5·508 (3) Å, respectively (Torardi, 1985).

Discussion

Our interpretation of experimental diffraction results must be compared with the two models (BG and MIZ) previously proposed to explain the continuous variation of x and q^*. The range of x itself is a matter of discussion. BG reported x values in the range 0·8–1·33, with an average multiplicity m near 2·5 in the range 0·8–1·20. It seems that BG determined the x value from the reacting compound concentrations (nominal value), but MIZ report that the range is restricted to 1·16–1·33 for $Ba_xTi_{8-2x}Ga_{2x}O_{16}$. Incomplete reaction on synthesis (unreacted TiO_2 is frequently present) would result in an actual x value differing from the nominal value, as was also shown by neutron diffraction studies of similar compounds by Cheary (1986). Our electron diffraction pattern (Fig. 1) closely resembles the $x = 1$ one in BG's Fig. 2(*b*), even concerning relative intensities. Therefore, we believe, as did MIZ, that BG considered a too large range of x. In this case, the narrow range of superlattice multiplicities m is not surprising. In particular, it is not necessary to introduce the softening of a rutile-like transverse acoustical mode of the framework to explain this tendency to obtain $m \simeq 2·5$.

The basic assumption of the MIZ model is that of isolated vacancies, so that x is necessarily greater than 1. These define a modulation wave parallel to the **b** axis with period $\mathbf{p} = m\mathbf{b}_{sub}$. For $x = 1·25$, the
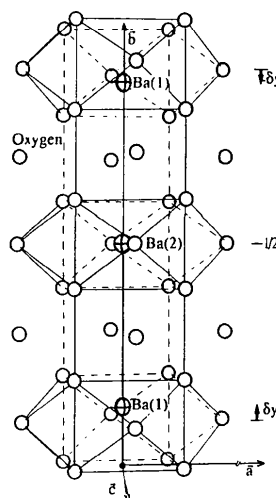

Fig. 5. The Ba environment in the tunnels of $Ba_{1.2}Ti_{6.8}Mg_{1.2}O_{16}$.

phase shift between the two cell tunnels $(0, y, 0)$ and $(\frac{1}{2}, y, \frac{1}{2})$ is such that vacancies form zigzag arrays perpendicular to the *b* axis in MIZ's model. Its main advantages are to provide a convenient way of indexing incommensurate diffraction patterns (in our case $q^* \simeq 0\cdot4\,b^*$) and to establish the relationship $x = 2$ $(1 - 1/m)$. Application of this relationship to our samples yields $1\cdot20 \le x \le 1\cdot24$ for crystals of the same batch $(0\cdot38 \le q^* \le 0\cdot40)$.

The Ba-vacancy ordering found in $Ba_{1\cdot2}Ti_{6\cdot8}Mg_{1\cdot2}O_{16}$ (this work) and $Ba_{1\cdot33}Ru_8O_{16}$ (Torardi, 1985) structure refinements and in $Ba_{1\cdot25}$ simulations (MIZ) agree with MIZ's model, if no phase shift between the modulation waves describing the two tunnels of a cell is considered. In this case, the width of the blocks of Ba planes is quite regular: three or four Ba planes in the range $1\cdot20 \le x \le 1\cdot33$, and follows the tooth-like pattern represented in Fig. 6. Our $m_0 = 5$ supercell is described by a wave of period $m = 2\cdot5$. Fig. 6, including $x = 1\cdot20$, $x = 1\cdot33$ (commensurate phases) and an intermediate case,

clearly shows that the $x = 1\cdot20$ cell is body centered and the $x = 1\cdot33$ one primitive. This result is also confirmed by our study of $Ba_{1\cdot33}Ti_{6\cdot67}Mg_{1\cdot33}O_{16}$ (Fanchon, Vicat & Hodeau, 1987). It can be added that the modulation waves between neighboring tunnels are not always in phase, since Pring *et al.* (1983) found another pattern in $K_{1\cdot33}Sb_{4\cdot89}Mg_{3\cdot11}O_{16}$.

BG described phases in the range $1\cdot20 < x < 1\cdot33$ by proper intergrowths of $m_0 = 5$ and $m_0 = 3$ commensurate superstructures. The two models look essentially the same: the tooth-like model also leads to $m_0 = 5$ and $m_0 = 3$ superstructures (Fig. 6*b*). They differ by a disordering of the block distribution in BG's model, whereas it is ordered in the tooth-like model.

The $x = 1\cdot20$ phase is fully ordered in both models (refinement *b* in Table 2). BG's observations and ours show the presence of microdomains for compositions close to $x = 1\cdot20$. BG proposed the occurrence of domains made of $Ba-[Ba-\square-Ba-\square-Ba]$ sequences and domains made of $\frac{1}{2}Ba-[(\frac{1}{2}Ba)-Ba-\square-Ba-(\frac{1}{2}Ba)]$ sequences in the $x = 1\cdot20$ phase. Our data collection was carried out on a crystal with $q^* = 0\cdot40\ (1)\ b^*$,

$\boxed{x = 1.2}(=6/5)$
$q = 0.40$
$m = 2.5$
$m_0 = 5$

$\boxed{x = 1.231}$
$q = 0.385$
$m = 2.6$

$\boxed{x = 1.33}(=4/3)$
$q = 0.33$
$m = 3$
$m_0 = 3$

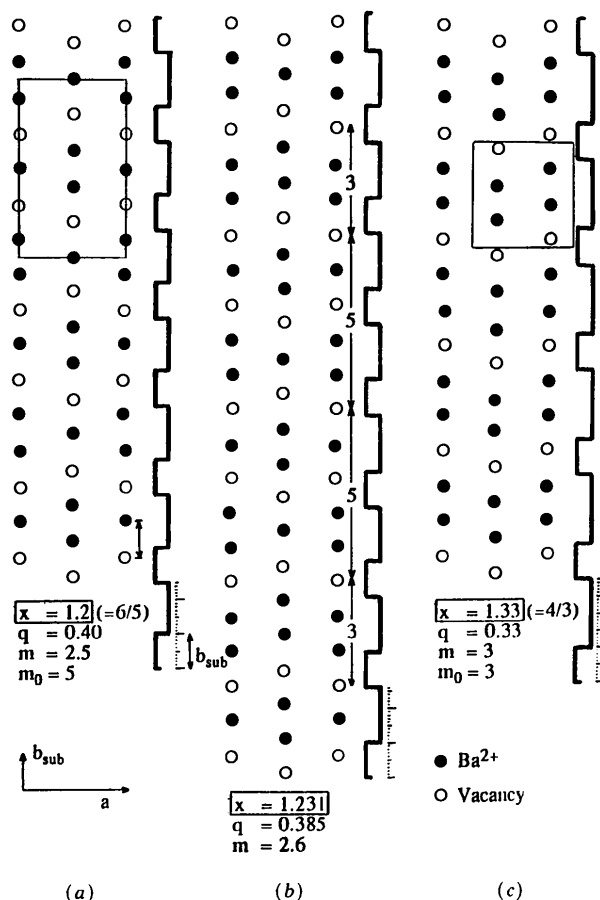● Ba^{2+}
○ Vacancy

(*a*)   (*b*)   (*c*)

Fig. 6. Projection of different $Ba/\square$-ordering schemes with associated modulation waves in the tunnels of $Ba_xTi_{8-x}Mg_xO_{16}$. (*a*) $x = 1\cdot20$, $m = 2\cdot5$, $m_0 = 5$; (*b*) $x = 1\cdot231$, $m = 2\cdot6$; (*c*) $x = 1\cdot33$, $m = 3$, $m_0 = 3$.
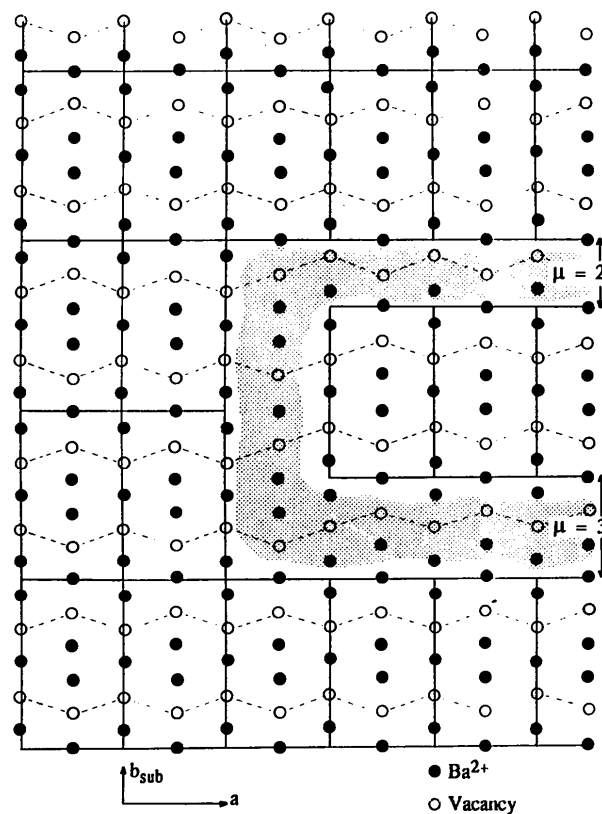

● Ba^{2+}
○ Vacancy

Fig. 7. Schematic projection of a *T*3-translated domain embedded in the *T*0 reference matrix. The shaded area corresponds to the perturbed region, *i.e.* domain wall. It can be seen that the zigzag pattern is preserved, but deformed. We have adopted the following rule to construct the figure: neither adjacent vacancies nor 3 adjacent Ba atoms can exist.

yielding 0·606, 0·030, 0·167 for n_0, n_1, n_2, respectively (with constraints $n_3 = n_2$, $n_4 = n_1$). These values suggest another type of disorder in this commensurate phase: inside large domains taken as reference ($T0$), there are smaller domains translated by $T2$ or $T3$ occupying 33% of the volume, and a small amount of domains translated by $T1$ and $T4$. The near absence of $T1$ and $T4$ domains can be interpreted by the fact that they cause much more perturbations at the domain walls. An example of a $T3$ domain is outlined in Fig. 7. It should be noted that these domains do not alter the global composition. We think that this kind of translated domain must be added to the tooth-like model for a complete description of most compounds in the range 1·0-1·33.

We think the domains found in $Ba_{1.2}Ti_{6.8}Mg_{1.2}O_{16}$ could be explained by the fact that domain walls are pinned by inhomogeneities of the Ti/Mg distribution in the framework. In the study of $BaRu_6O_{12}$ (Torardi, 1985), the domain problem did not seem to arise; we suggest that its absence is due to the mixed-valence character of the framework cation Ru.

BG interpret the ionic conductivity by a displacement of domain walls, that is a collective movement of Ba^{2+} ions. A pinning of the domain walls on Ti/Mg inhomogeneities would obviously result in poor conductivity. The disorder problem has been addressed differently in the absence of three-dimensional correlations. Beyeler, Pietronero & Strässler (1980) use a short-range-order model to calculate diffuse profiles in $K_{1.54}Ti_{7.23}Mg_{0.77}O_{16}$ and estimate the correlation length to be about 35 Å along the tunnel axis.

The X-ray data were collected within the 'Groupe Grenoblois de Diffractométrie'.

References

BEYELER, H. U., PIETRONERO, L. & STRÄSSLER, S. (1980). *Phys. Rev. B*, **22**, 2988-3000.
BEYELER, H. U. & SCHÜLER, C. (1980). *Solid State Ionics*, **1**, 77-86.
BURSILL, L. A. & GRZINIC, G. (1980). *Acta Cryst.* **B36**, 2902-2913.
BYSTRÖM, A. & BYSTRÖM, A. M. (1950). *Acta Cryst.* **3**, 146-154.
CHANG, F. M. & JANSEN, M. (1986). *Rev. Chim. Minér.* **23**, 48-54.
CHEARY, R. W. (1986). *Acta Cryst.* **B42**, 229-236.
COWLEY, J. M. & MOODIE, A. F. (1957). *Acta Cryst* **10**, 609-619.
DRYDEN, J. S. & WADSLEY, A. D. (1958). *Trans. Faraday Soc.* **54**, 1574-1580.
ENRAF-NONIUS (1979). *Structure Determination Package*. Enraf-Nonius, Delft, The Netherlands.
FANCHON, E., VICAT, J. & HODEAU, J.-L. (1987). In preparation.
HODEAU, J.-L., MAREZIO, M., SANTORO, A. & ROTH, R. S. (1983). *Solid State Ionics*, **9 & 10**, 77-82.
International Tables for X-ray Crystallography (1974). Vol. IV. Birmingham: Kynoch Press. (Present distributor D. Reidel, Dordrecht, The Netherlands.)
MIJLHOFF, F. C., IJDO, D. J. & ZANDBERGEN, H. W. (1985). *Acta Cryst.* **B41**, 98-101.
O'KEEFE, M. A. (1980). *SHRLI80F* (*Simulated High-Resolution Lattice Image*) programs. Univ. of Cambridge, England.
POST, J. E., VON DREELE, R. B. & BUSECK, P. R. (1982). *Acta Cryst.* **B38**, 1056-1065.
PRING, A., SMITH, D. J. & JEFFERSON, D. A. (1983). *J. Solid State Chem.* **46**, 373-381.
SHANNON, R. D. (1976). *Acta Cryst* **A32**, 751-767.
TORARDI, C. C. (1985). *Mater. Res. Bull.* **20**, 705-713.
VICAT, J., FANCHON, E., STROBEL, P. & TRAN QUI, D. (1986). *Acta Cryst.* **B42**, 162-167.
WATELET, H., BESSE, J.-P., BAUD, G. & CHEVALIER, R. (1982). *Mater. Res. Bull.* **17**, 863-871.
WEBER, H.-P. & SCHULZ, H. (1983). *Solid State Ionics*, **9 & 10** 1337-1340.
WOLFERS, P. (1987). In preparation.

Electron Density in Chromium Sulfate Pentahydrate

BY T. P. VAALSTA AND E. N. MASLEN

Crystallography Centre, University of Western Australia, Nedlands, Western Australia 6009, Australia

Abstract

The structure of the title compound has been refined using an accurate set of X-ray data: $CrSO_4.5H_2O$, $M_r = 238.1$, triclinic, $P\bar{1}$, $a = 6.188 (1)$, $b = 10.929 (2)$, $c = 6.039 (1)$ Å, $\alpha = 82.40 (2)$, $\beta = 107.77 (1)$, $\gamma = 102.71 (2)°$, $V = 378.46 (2)$ Å^3, $Z = 2$, $D_x = 2.09$ g cm^{-3}, Mo $K\alpha$, $\lambda = 0.71069$ Å, $\mu = 17.03$ cm^{-1}, $F(000) = 244$, $T = 298$ K, $R = 0.039$ for 7958 unique reflections. Difference electron-density maps are evaluated for sections through two Cr nuclei containing four water O atoms and ligating sulfate O atoms. The anisotropy of the deformation density $\Delta\rho$ around the Cr nuclei is related to unequal occupancy of the $3d$ metal orbitals, as expected in view of the Jahn-Teller distortion in the structure. The density